SurfelSplat: Learning Efficient and Generalizable Gaussian Surfel Representations for Sparse-View Surface Reconstruction

Chensheng Dai[*] **Shengjun Zhang**[*] **Min Chen, Yueqi Duan**[†]
Tsinghua University
{dcs23, zhangsj23,cm22}@mails.tsinghua.edu.cn, duanyueqi@tsinghua.edu.cn

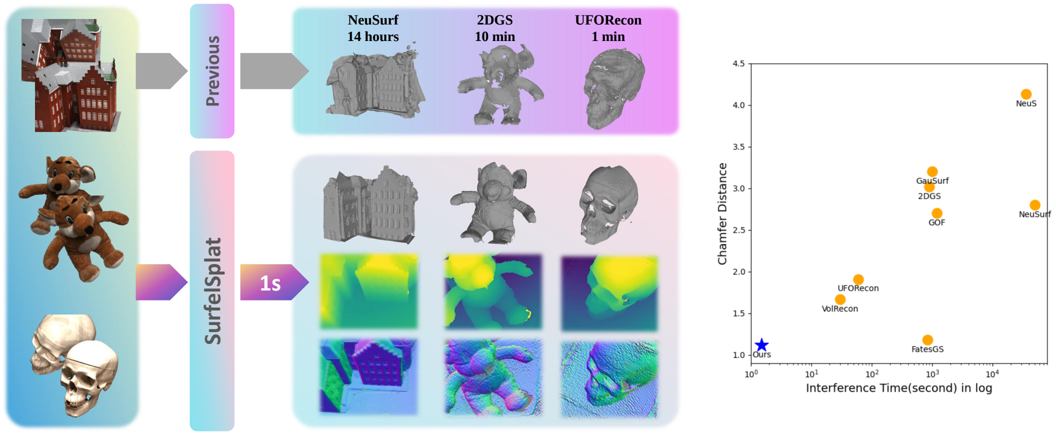

(a) Visualization and performance of our framework

(b) Performance and runtime comparison

Figure 1: Our method delivers state-of-the-art surface reconstruction with ultra-fast inference speed. (a) Framework visualization: Given an image pair, our approach regresses Gaussian radiance fields capturing fine geometric details in just 1 second. (b) Quantitative comparisons: Our method achieves superior reconstruction accuracy while maintaining the fastest runtime among existing approaches.

Abstract

3D Gaussian Splatting (3DGS) has demonstrated impressive performance in 3D scene reconstruction. Beyond novel view synthesis, it shows great potential for multi-view surface reconstruction. Existing methods employ optimization-based reconstruction pipelines that achieve precise and complete surface extractions. However, these approaches typically require dense input views and high time consumption for per-scene optimization. To address these limitations, we propose SurfelSplat, a feed-forward framework that generates efficient and generalizable pixel-aligned Gaussian surfel representations from sparse-view images. We observe that conventional feed-forward structures struggle to recover accurate geometric attributes of Gaussian surfels because the spatial frequency of pixel-aligned primitives exceeds Nyquist sampling rates. Therefore, we propose a cross-view feature aggregation module based on the Nyquist sampling theorem. Specifically, we first adapt the geometric forms of Gaussian surfels with spatial sampling rate-guided low-pass filters. We then project the filtered surfels across all input views to obtain cross-view feature correlations. By processing these correlations through a

[*] Equal contribution

[†] Corresponding author.

39th Conference on Neural Information Processing Systems (NeurIPS 2025).

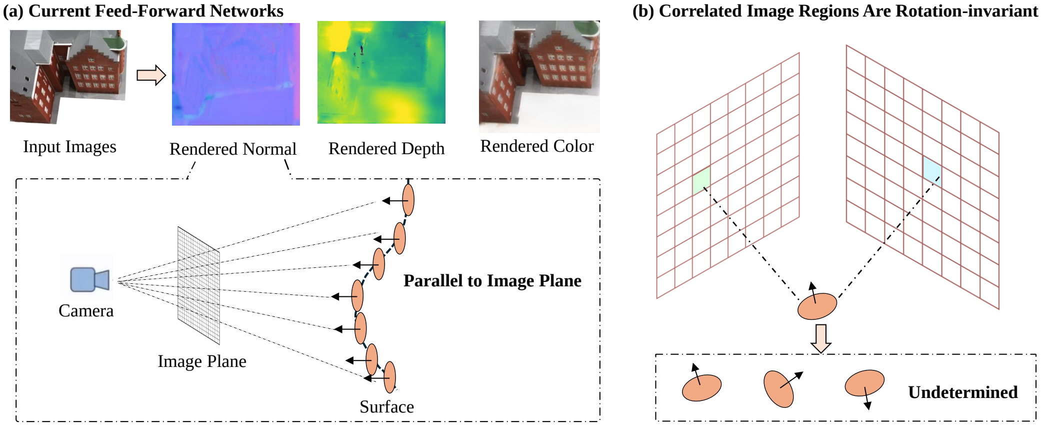

Figure 2: Experimental Observation. (a) Current feed-forward networks generate geometrically inaccurate Gaussian radiance fields. (b) The correlated image regions of pixel-aligned Gaussian surfels exhibit rotation invariance, limiting the network's ability to accurately infer surface orientations.

specially designed feature fusion network, we can finally regress Gaussian surfels with precise geometry. Extensive experiments on DTU reconstruction benchmarks demonstrate that our model achieves comparable results with state-of-the-art methods, and predict Gaussian surfels within 1 second, offering a 100× speedup without costly per-scene training.

1 Introduction

Reconstructing accurate surfaces from multi-view images remains a fundamental challenge in computer vision. Previous methods focus on Multi-View Stereo [1, 2] techniques to capture geometric details from multi-view images. Recent advancements of neural implicit representations [3, 4, 5, 6, 7, 8, 9, 10, 11, 12, 13] have demonstrated significant progress in recovering smooth and complete surface. However, these approaches typically struggle to extract precise surfaces in terms of sparse viewpoints. While following works [6, 7, 14, 15] have shown promise in sparse-view reconstruction, they generally require per-scene optimization with high time consumption. More recently, 3D Gaussian Splatting (3DGS) [16] has recently drawn increasing attention due to its rapid rendering speed and high visual fidelity. To enhance the surface alignment capabilities of Gaussian primitives, recent approaches [17, 18, 19, 20, 21] have modified the geometric shape of Gaussian representations to better conform to actual surfaces. For instance, 2D Gaussian Splatting (2DGS) [18] transforms 3D Gaussian primitives into 2D Gaussian surfels to maintain improved view-consistent geometry. While 3DGS-based methods succeed in precise surface extraction, they tend to overfit to the camera when presented with limited viewpoint information (*i.e.*, as few as two images), resulting in geometric collapse.

To circumvent per-scene optimization while ensuring generalizable and efficient scene reconstruction, several feed-forward networks [22, 23, 24, 25, 26, 27, 28, 29] have been proposed to directly regress 3D Gaussian parameters from sparse-view input images. These approaches predict the depth map and appearance attributes of pixel-aligned Gaussian primitives from cross-view image features. Current feed-forward frameworks achieve superior performance in fast and generalizable scene reconstruction for novel view synthesis. Therefore, an intuitive approach is to apply the current feed-forward networks for parameter prediction of 2D Gaussian surfels. However, as shown in Figure 2, typical methods such as MVSplat [24] fail to generate surfels with accurate geometry, where the normal vectors of surfels cannot be precisely recovered. The Gaussian surfels tend to orient parallel to the image plane rather than aligning with the actual surface geometry. As shown in Figure 2(b), Gaussian surfels predicted by these networks only cover the area of a single pixel. Consequently, the corresponding image regions relevant to surfel attributes cannot provide sufficient supervisory information to accurately learn the covariance of Gaussian surfels.

In this paper, we first analyze this phenomenon from the perspective of the Nyquist sampling theorem. Our key insight is that the failure to generate surface-aligned primitives is because the spatial frequency of pixel-aligned Gaussian surfels exceeds the Nyquist sampling rate, thus violating the fundamental signal processing principles. To trackle this challenge, we introduce SurfelSplat, a novel feed-forward framework to regress 2D Gaussian radiance field with precise geometry guided by Nyquist theorem. Our method dynamically modulates the geometric forms of diverse Gaussian surfels in the frequency domain and correlates pixel regions across multiple input views that effectively contribute to Gaussian geometric feature learning. We subsequently develop a feature aggregation network that leverages image features from these identified regions to enhance the original Gaussian image features, thereby yielding accurate Gaussian surfel representations with improved geometric fidelity. Our contributions are summarized as follows:

- We propose SurfelSplat, a feed-forward framework that regresses 2D Gaussian surfels directly from sparse-view images for surface reconstruction.
- We conduct a detailed analysis of why current feed-forward frameworks fail to generate geometrically-accurate Gaussian primitives and introduce Nyquist theorem-guided Gaussian surfel adaptations and feature aggregations to achieve superior geometric properties of the scene.
- Experimental results demonstrate the effectiveness of our method. SurfelSplat generates surface-aligned Gaussian radiance fields with high efficiency and accurate geometry.

2 Related Work

2.1 Neural Implicit 3D Representation

Neural Radiance Fields (NeRF) represent scenes through implicit radiance fields, with optimization processes dependent on volumetric rendering [30, 31, 32, 33, 34, 35, 36, 37, 38, 39, 40, 41, 42, 43, 44, 45, 46, 47, 48, 49]. For surface reconstruction, NeuS [3] pioneered scene representation using implicit Signed Distance Functions (SDFs) [5, 11, 12, 50]. The inherent continuity of MLP-based SDFs ensures smooth and accurate extracted meshes. Subsequent research has enhanced performance in sparse-view settings: VolRecon [51] integrates multi-scale feature extraction with geometry-aware regularization to recover 3D surfaces from limited viewpoints; NeuSurf [6] combines differentiable rendering with adaptive surface extraction techniques, enabling high-fidelity recovery of complex geometries; and UFORecon [8] employs an uncertainty-aware fusion optimization framework that leverages probabilistic feature correspondence and adaptive confidence weighting for robust surface reconstruction. However, the inherent complexity of volumetric rendering typically requires several hours of computation per scene.

2.2 Neural Explicit 3D Representation

Beyond neural implicit representations, 3D Gaussian Splatting (3DGS) has achieved remarkable progress in 3D scene reconstruction, delivering photorealistic rendering quality with high rendering speed [16, 52, 53, 54, 55, 56, 57, 58]. Two primary approaches have emerged for accurate surface extraction. The first enhances primitives to better fit surfaces: SuGaR [17] models 3D Gaussians as 2D pieces by incorporating flat and signed-distance regularization terms; 2DGS [18] and Gaussian Surfels [19] transform 3D Gaussian primitives into 2D surfels, with 2DGS proposing depth and normal consistency constraints to align surfels more accurately with surfaces. The second approach combines implicit representations to guide 3DGS training: NeuSG [59] integrates NeRF and 3DGS to recover complex 3D surfaces through differentiable optimization that preserves both local details and global structure; GSDF [21] employs a two-branch framework to simultaneously optimize SDF and Gaussian fields, allowing mutual enhancement to capture better geometric details. However, these methods require dense views to obtain smooth and complete surfaces due to the lack of scene data priors.

2.3 Generalizable Feed-forward Networks

The aforementioned optimization-based approaches have demonstrated strong performance in 3D reconstruction tasks, yet they typically require expensive per-scene training. More recently, feed-forward networks have emerged as a promising paradigm for generalizable 3D scene reconstruction.

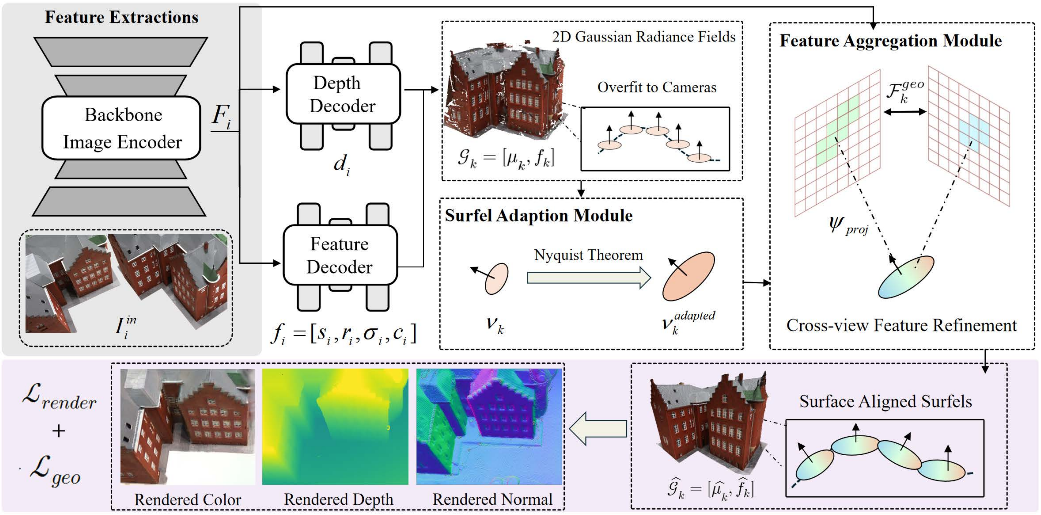

Figure 3: Pipeline. Given an image pair, our method first extracts initial image features using a backbone image encoder. We then predict Gaussian features and depth maps of the scene. Since 2D radiance fields are geometrically inaccurate, we apply Nyquist theorem-guided surfel adaptation to each surfel. In the feature aggregation module, we project the adapted surfels across views to identify image regions containing relevant geometric information. After refining the image features with these related regions, we regress the Gaussian radiance fields again to obtain accurate representations.

These models learn rich priors from large-scale datasets, enabling the reconstruction process to be accomplished through a single feed-forward inference. pixelNeRF [47] pioneered a feature-based framework that leverages encoded features to render novel views. Building upon Gaussian primitives as the fundamental representation, Splatter Image [22] and GPS-Gaussian [53] have achieved notable progress by predicting Gaussian parameters for object-level reconstruction. pixelSplat [23] further advanced this direction by regressing pixel-aligned Gaussian primitives, effectively incorporating epipolar geometry and depth estimation. MVSplat [24] enhances geometric quality by extracting cost volumes as cross-view features, which facilitates fast and accurate depth prediction. However, existing feed-forward methods predominantly target 3D reconstruction tasks such as novel view synthesis. Their potential for surface reconstruction—where significantly higher precision in Gaussian primitives is required—remains largely unexplored.

3 Methods

We present SurfelSplat, a feedforward framework for predicting 2D Gaussians with accurate geometric reconstruction, principled by the Nyquist sampling theorem (Figure 3). Our approach begins by predicting Gaussian centers and their associated attributes, followed by a surfel adaptation module that optimizes Gaussian primitives in the frequency domain. We then introduce a feature aggregation module that refines Gaussian representations by exploiting cross-view feature correlations. These refined features are subsequently utilized to regress surface-aligned 2D Gaussian radiance fields. In Section 3.1, we present a comprehensive analysis of spatial frequency characteristics and sampling rates for Gaussian surfels. Section 3.2 details our Nyquist-guided surfel adaptation and image feature aggregation modules, along with their corresponding network architectures. Our SurfelSplat is illustrated in Algorithm 1.

3.1 Sensitivity to Sampling Rates for Pixel-Aligned Gaussian Surfels

To overcome the limitations inherent in current pixel-aligned feedforward approaches, we initially examine the spatial sampling frequency within multi-camera systems and establish a methodology for computing the spatial frequency of individual 2D Gaussian primitives.

Algorithm 1 SurfelSplat: Nyquist Sampling-Guided Gaussian Feature Aggregation

```
Input: Multi-view images $\mathcal{I} = \{\mathbf{I}_i\}_{i=1}^N$, camera parameters $\mathcal{P} = \{\mathbf{P}_i\}_{i=1}^N$, $f_x$ and $f_y$
Output: Gaussian parameters $\{\mu_k, \mathbf{r}_k, \mathbf{s}_k, \sigma_k, \mathbf{c}_k\}$ for each primitive $k$
$\mathcal{F} \leftarrow \Phi_{image}(\mathcal{I}, \mathcal{P})$
$\mu_i \leftarrow \psi_{unproj}(\Phi_{depth}, \mathbf{P}_i), \quad f_i \leftarrow \Phi_{attr}(F_i) \quad i = 1, 2, \cdots, N$
for $i \leftarrow 1$ to $N$ do
    $d_k^i \leftarrow \psi_{proj}(\mathcal{G}_k, \mathbf{P}_i)$
    $\hat{\nu}_k^i \leftarrow \frac{f_x f_y}{(d_k^i)^2}$
end for
$\hat{\nu}_k \leftarrow \max_i \hat{\nu}_k^i$
$\mathcal{G}_k^{low} \leftarrow exp(-\frac{\hat{\nu}_k^2 u^2}{2s^2} - \frac{\hat{\nu}_k^2 v^2}{2s^2}), \quad \hat{\mathcal{G}}_k^{adapted} \leftarrow \mathcal{G}_k \otimes \mathcal{G}_k^{low}$
$\mathcal{F}_k^{geo} \leftarrow \psi_{proj}(\mathcal{F}, \mathcal{P}, \hat{\mathcal{G}}_k^{adapted})$
$\mathbf{F}_k^{refined} \leftarrow \Phi_{refine}(\mathcal{F}_k^{geo}) + \mathbf{F}_k$
$\hat{\mathbf{f}}_k \leftarrow [\hat{\mathbf{s}}_k, \hat{\mathbf{r}}_k, \hat{\sigma}_k, \hat{\mathbf{c}}_k] = \Phi_{attr}(\mathbf{F}_k^{refined})$
```

3.1.1 Nyquist Sampling Theorem

The Nyquist Sampling Theorem [60] represents a cornerstone principle in signal processing. For precise reconstruction of a continuous signal from its discrete samples, the following criteria must be met:

Nyquist Conditions *The continuous signal must be band-limited with bandwidth ν, and the spatial sampling rate $\hat{\nu}$ must be at least twice the signal bandwidth:$\hat{\nu} \geq 2\nu$.*

The Nyquist sampling theorem establishes the fundamental relationship between spatial signals and their corresponding sampling frequencies. In this work, we exploit the Nyquist criterion to learn local image features that significantly improve the reconstruction of fine-grained geometric scene details.

3.1.2 Spatial Sampling Rates in Multi-Camera Systems

For a single-camera system, the sampling interval in the image plane is determined by the pixel area. When projected into 3D space, this sampling interval corresponds to the area occupied on the surface manifold. For an image with focal lengthsf_x and f_y(expressed in pixel units), the sampling interval in screen space is unity. Consider a unit area element dA_{xy} in screen space and its corresponding surface area coverage dA_{uv}. The sampling rate in 3D space can then be derived as:

$$\hat{\nu}_{sampling} = \frac{dA_{xy}}{dA_{uv}} \tag{1}$$

The relationship between these two parameter spaces is given by $dA_{xy} = |\mathbf{J}| du \cdot dv$, where $|\mathbf{J}|$ represents the determinant of Jacobian matrix: $\mathbf{J} = \frac{\partial \mathbf{P}_{image(x,y)}}{\partial \mathbf{X}_{camera}} \cdot \frac{\partial \mathbf{X}_{camera}}{\partial \mathbf{X}_{world}} \cdot \frac{\partial \mathbf{X}_{world}}{\partial (u,v)}$. By evaluating the spatial projection relationship that governs the projection process, we obtain the sampling frequency for a given spatial primitive:

$$\hat{\nu}_{sampling} = |\mathbf{J}| = \frac{f_x f_y}{d^2} \tag{2}$$

where d denotes the corresponding depth value. The detailed mathematical derivation is provided in the Appendix B.1. For a multi-camera system, the spatial sampling frequency is computed across all cameras. We define the overall sampling frequency for a Gaussian primitive p_k as the maximum frequency among all views:

$$\hat{\nu}_k = \max \left(\{\mathbb{V}_i(p_k) \cdot |J_i|\}_{i=1}^N \right) \tag{3}$$

where N represents the number of cameras and $\mathbb{V}_i$ denotes the visibility function. If the primitive is visible to the i-th camera, $\mathbb{V}_i$ returns 1, otherwise 0. Specifically, our choice of using the maximum sampling frequency as the overall frequency (Equation 3) is motivated by Equation 7 of Mip-Splatting [54]. The key insight of Mip-Splatting is that for accurate reconstruction, we need to ensure that each

3D Gaussian primitive satisfies the Nyquist sampling criterion for **at least one camera view** where it is visible. This is because if a primitive can be accurately reconstructed from at least one view, we have captured its essential geometric information.

3.1.3 Spatial Frequency of 2D Gaussian Primitives

Given a spatial surfel, the spatial frequency can be calculated through spatial Fourier transform derivation $|\hat{G}(\mathbf{k})|$. Since the Gaussian function contains over 95% of its energy within ± 2 standard deviations, when considering a Gaussian with two standard deviations as the surfel size, we can obtain the frequencies along the tangent vector directions $\mathbf{t}_u$ and $\mathbf{t}_v$ in the 2D Gaussian surfel via $|\hat{G}(\mathbf{t}_u)|$ and $|\hat{G}(\mathbf{t}_v)|$, respectively. The detailed derivation can be found in Appendix B.2.

Consequently, along the $\mathbf{t}_u$ direction, the frequency is $\omega_u = \frac{2}{s_u}$ (and analogously, $\omega_v = \frac{2}{s_v}$ for the $\mathbf{t}_v$ direction). Accounting for the 2π periodic normalization of the Fourier transform, the spatial frequency of the Gaussian primitive along each tangent vector can be expressed as:

$$\nu_u = \frac{1}{\pi s_u}, \quad \nu_v = \frac{1}{\pi s_v} \tag{4}$$

For Gaussian primitives that fail to satisfy the Nyquist criterion, the spatial signal cannot be perfectly reconstructed. In such cases, the network tends to predict spatial parameters (e.g., covariance) with considerable stochasticity, resulting in surfels that are misaligned with the actual surface geometry.

3.2 Surfel Prediction with Nyquist Theorem-Guided Feature Aggregation

Having established the methodology for calculating sampling rates and spatial primitive frequencies, we proceed to design modules that enable Gaussian primitive predictions to adhere to the Nyquist sampling criterion. Specifically, we perform Gaussian surfel adaptation in the frequency domain and employ cross-view feature aggregation to regress primitives with enhanced geometric detail fidelity.

3.2.1 Nyquist Theorem-Guided Gaussian Surfel Adaptation

We aim to constrain the maximum frequency of $\mathcal{G}_k$ according to the spatial sampling rates. We propose an adaptive surfel adaptation module operating in the frequency domain. Specifically, we achieve this by passing 2D Gaussian primitives through an adaptive Gaussian low-pass filter:

$$\hat{\mathcal{G}}_k^{\text{adapted}}(\mathbf{x}) = (\mathcal{G}_k \otimes \mathcal{G}_k^{\text{low}})(\mathbf{x}), \quad \mathcal{G}_k^{\text{low}}(x) = e^{-\frac{\hat{\nu}_k^2 u^2}{2s^2} - \frac{\hat{\nu}_k^2 v^2}{2s^2}} \tag{5}$$

Here, s is a scalar hyperparameter (default value is 1), and each Gaussian filter is designed according to the specific frequency bound $\hat{\nu}_k$. We then adaptively modify the transformation matrix of the 2D Gaussian primitive $\mathbf{H}_k^{\text{adapted}}$ as the scaling matrix changes:

$$\mathbf{H}_k^{\text{adapted}} = \begin{bmatrix} s_u\sqrt{1+\frac{s^2}{\hat{\nu}_k^2}}\mathbf{t}_u & s_v\sqrt{1+\frac{s^2}{\hat{\nu}_k^2}}\mathbf{t}_v & \mathbf{0} & \mathbf{p}_k \\ 0 & 0 & 0 & 1 \end{bmatrix} = \begin{bmatrix} \mathbf{RS}_k^{\text{adapted}} & \mathbf{p}_k \\ \mathbf{0} & 1 \end{bmatrix} \tag{6}$$

where $\mathbf{S}_k^{\text{adapted}}$ is the adapted scaling matrix, and the transformation matrix $\mathbf{H}_k^{\text{adapted}}$ completely characterizes the 2D Gaussian representation, incorporating the effects of the low-pass filter.

Theoretical Nyquist Criterion Verification Prior to adaptation, whether all primitives satisfy the Nyquist criterion cannot be determined. After adaptation, the spatial frequency can be constrained by setting $s_u > \frac{2}{\pi}$:

$$\nu_k = \frac{1}{s_u\pi\sqrt{1+\frac{1}{\hat{\nu}_k^2}}} < \frac{\hat{\nu}_k}{s_u\pi} < \frac{\hat{\nu}_k}{2} \tag{7}$$

Regardless of how the spatial sampling rates vary, the Nyquist criterion is consistently satisfied.

3.2.2 Nyquist Theorem-Guided Gaussian Feature Aggregation

Gaussian Parameters Initialization Given N input images $\mathcal{I} = \{\mathbf{I}_i\} \in \mathbb{R}^{N\times H\times W\times 3}$ and corresponding camera parameters $\mathcal{P} = \{\mathbf{P}_i\}, \mathbf{P}_i = \mathbf{K}_i[\mathbf{R}_i|\mathbf{t}_i]$, we first use epipolar transformers to extract rough image features, and use cost volumes between perspective pairs to extract geometric interrelationships. We then concatenate these features to obtain our initial image features:

$$\mathcal{F} = \Phi_{initial}(\mathcal{I}), \mathcal{F} = \{\mathbf{F}_i\} \in R^{N\times W\times H\times C} \tag{8}$$

where $\Phi_{initial}$ is the image feature extraction backbone. In conventional feedforward frameworks, cross-view features are fed into two distinct regression networks Φ_{depth} and Φ_{attr} to predict depth $\mathbf{d}_i$ and Gaussian attributes $\mathbf{f}_i = [\mathbf{s}_i, \mathbf{r}_i, \sigma_i, \mathbf{c}_i]$:

$$\mathbf{d}_i = \Phi_{depth}(\mathbf{F}_i) \in \mathbb{R}^{HW}, \mu_i = \psi_{unproj}(\mathbf{d}_i, \mathbf{P}_i) \in \mathbb{R}^{HW\times 3}, \mathbf{f}_i = \Phi_{attr}(\mathbf{F}_i) \in \mathbb{R}^{HW\times C_{attr}} \tag{9}$$

where ψ_{unproj} denotes the unprojection process.

Cross-view Gaussian Feature Aggregation Given the frequency distribution in space, we perform Gaussian surfel adaptations for each primitive $\hat{\mathcal{G}}_k^{\text{adapted}}(\mathbf{x}) = (\mathcal{G}_k \otimes \mathcal{G}_k^{\text{low}})(\mathbf{x})$. Within our framework, we project 2D Gaussian primitives back to all viewpoints to extract the set of image features required for refinement. With lower frequency, primitives tend to occupy more pixels related to Gaussian attributes regression. The image regions $\mathcal{R}_k$ associated with $\hat{\mathcal{G}}_k^{\text{adapted}}$ are defined by:

$$\mathcal{R}_k^i = \{\mathbf{x} = (i,j) \in \mathbb{Z}^2 : \hat{\mathcal{G}}_k^{\text{adapted}}(i,j;m) > \epsilon\}, \quad \mathcal{R}_k = \bigcup_{i=1}^{N} \mathcal{R}_k^i \tag{10}$$

where $\hat{\mathcal{G}}_k^{\text{adapted}}(i,j;m)$ represents the Gaussian value of primitive $\hat{\mathcal{G}}_k^{\text{adapted}}$ splatted onto the m^{th} view at pixel (i,j).

We can then identify image features associated with the geometric information of primitive $\mathcal{G}_k$:

$$\mathcal{F}_{i,k}^{\text{geo}} = \{\mathbf{F}_k^i(i,j), (i,j) \in \mathcal{R}_k^i\}, \quad \mathcal{F}_k^{\text{geo}} = \bigcup_{i=1}^{N} \mathcal{F}_{i,k}^{\text{geo}} \tag{11}$$

Gaussian Prediction with Refined Feature As features in $\mathcal{F}_k^{\text{geo}}$ are essential for accurate geometry learning of our Gaussian representation $\mathcal{G}_k$, we implement a feature refinement architecture with cross-attention transformations to enhance the initial image feature $\mathbf{F}_k$. The query, key, and value composition is specifically designed to enable cross-attention interaction for a Gaussian primitive $\mathcal{G}_k$ as $\hat{F}_k = \Phi_{\text{Att}}(Q, K, V)$:

$$Q = h_Q(\mathbf{F}_k), \quad K = h_K(\mathcal{F}_k^{geo}), \quad V = h_V(\mathcal{F}_k^{\text{geo}}) \tag{12}$$

We then employ a standard feed-forward architecture in the transformer:

$$\mathbf{F}_k^{\text{refined}} = \Phi_{\text{FFN}}(\hat{\mathbf{F}}_k) + \mathbf{F}_k \tag{13}$$

Finally, we predict geometry-aware pixel-aligned 2D Gaussian primitives with the refined feature per view $\mathbf{F}_i^{\text{refined}} = \{\mathbf{F}_k^{\text{refined}}, \mathcal{G}_k \subset \mathcal{I}_i\}$ using the same Gaussian head as in Equation 9:

$$\hat{\mathbf{f}}_i = [\hat{\mathbf{s}}_i, \hat{\mathbf{r}}_i, \hat{\sigma}_i, \hat{\mathbf{c}}_i] = \Phi_{\text{attr}}(\mathbf{F}_i^{\text{refined}}) \in \mathbb{R}^{HW\times C_{\text{attr}}} \tag{14}$$

3.3 Loss Design

Our loss function comprises two parts: rendering loss and geometric loss. The rendering loss $\mathcal{L}_{render} = \mathcal{L}_{RGB} + \lambda_{LPIPS}\mathcal{L}_{LPIPS}$ employs mean square error along with LPIPS loss. For geometric loss, we use depth and normal continuity functions to align surfels to the surface: $\mathcal{L}_{align} = \sum_i \omega_i(1 - n_i^T N)$. Furthermore, we incorporate depth and normal mean square error: $\mathcal{L}_{geo} = \lambda_{align}\mathcal{L}_{align} + \lambda_d\mathcal{L}_d + \lambda_n\mathcal{L}_n$. Our complete loss function is formulated as:

$$\mathcal{L} = \mathcal{L}_{render} + \lambda_{geo}\mathcal{L}_{geo} \tag{15}$$

4 Experiments

To demonstrate the effectiveness of our method, we conduct experiments on DTU benchmarks [61] and compare the reconstruction accuracy and evaluation efficiency with state-of-the-art methods. Additionally, we provide a detailed analysis of the geometric properties from the perspective of the Nyquist sampling criterion to further validate our approach. In the ablation study, we analyze the effectiveness of each component of our method.

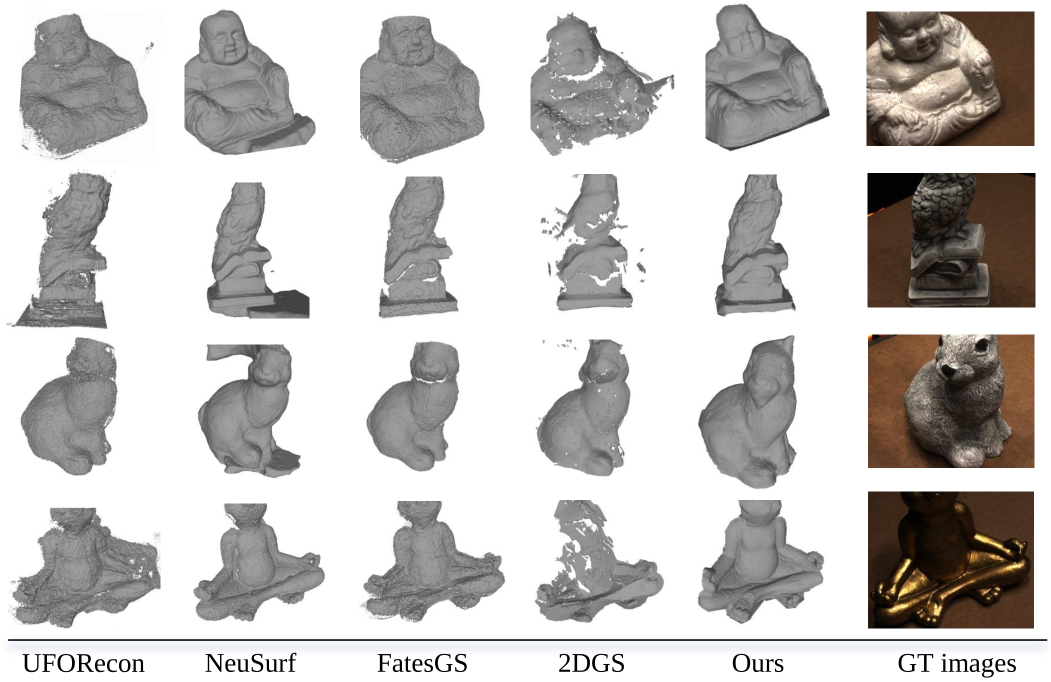

Figure 4: Qualitative Comparison of Surface Reconstruction with Sparse Views on DTU Benchmarks.

4.1 Experimental Setup

Datasets. We evaluate our method on the DTU dataset. DTU consists of 128 scenes, with 15 scenes designated for testing. We assess reconstruction accuracy using Destination to Source (D2S) Chamfer Distance as the evaluation metric. The investigated experimental setting is sparse-view reconstruction with 2 input views. Input images are downsampled to a resolution of 256×320 pixels.

Implementation Details. Our implementation is built upon the pixelSplat [23] framework. The training process consists of two stages: first, we train our model on RealEstate10K [62] for 300,000 iterations, followed by fine-tuning on the DTU dataset for 2,000 iterations. The hyperparameter s in Equation 5 is set to 1. All experiments reported in this paper were conducted on a single NVIDIA RTX A6000 GPU using the Adam optimizer.

4.2 Comparisons

Sparse view surface reconstruction. As shown in Table 1, our SurfelSplat exhibits the best mean D2S reconstruction Chamfer distance (CD) performance compared to other state-of-the-art surface reconstruction methods. As illustrated in Figure 4, our method presents superior global geometry and exhibits enhanced surface details. In contrast to UFORecon [8], which can only produce coarse global geometry, our method demonstrates improved global surface smoothness. We can also refine local details that would be ignored by methods like 2DGS [18], which delivers coarse and incomplete surfaces. Additional experimental results on the BlendedMVS [63] dataset are presented in Appendix C.4.

Efficiency. We conduct efficiency studies on all tested scenes for the sparse-view reconstruction methods mentioned above. As highlighted in Table 2, we compare the mean inference time on DTU benchmarks. All experiments are conducted on the same device.

For neural implicit methods that require per-scene training, convergence requires significantly long training times. Neural explicit training methods greatly reduce training time consumption, but still require approximately 10 minutes to obtain the Gaussian radiance fields. Most recent implicit methods have successfully compressed the inference time to the 1-minute level. However, our method shows the best efficiency with a single feed-forward process that takes only seconds.

Table 1: The quantitative comparison results of Chamfer Distance (CD↓) on DTU dataset. The best results are in **bold**, the second best are underlined.

ID	24	37	40	55	63	65	69	83	97	105	106	110	114	118	122	Mean
NeuS [3]	4.69	4.72	4.03	4.58	4.71	2.01	4.83	3.94	4.31	2.61	1.63	6.48	1.44	5.69	6.34	4.13
NeuSurf [6]	1.96	3.73	2.35	**0.82**	**1.07**	2.51	0.87	1.21	1.15	1.13	1.06	1.23	**0.41**	0.92	1.13	1.44
VolRecon [51]	1.41	3.24	1.76	1.43	1.66	2.25	1.42	1.81	1.54	1.26	1.52	1.53	0.99	1.54	1.75	1.67
UFORecon [8]	1.15	2.42	1.67	2.55	1.90	2.73	1.55	1.49	2.16	0.95	2.22	1.98	1.40	2.11	2.32	1.91
2DGS [18]	2.29	2.63	2.33	1.23	3.69	4.71	2.64	3.94	3.55	3.92	3.95	2.68	2.37	3.15	2.21	3.02
GausSurf [19]	4.22	5.69	4.32	3.98	4.93	2.81	4.67	5.52	4.98	3.61	4.11	5.43	2.98	3.66	4.55	4.36
FatesGS [64]	**0.77**	2.35	**1.43**	1.00	1.31	2.06	**0.85**	1.24	**1.06**	0.83	1.22	**0.58**	0.64	0.99	1.32	1.18
Ours	1.23	**1.69**	1.63	0.90	1.24	**1.14**	1.12	**1.18**	1.13	**0.79**	**0.84**	1.02	0.98	**0.84**	**1.04**	**1.12**

Table 2: Comparisons with reconstruction efficiency.

Method	Interference Time
NeuS	$10_{\pm 0.5}$ hours
NeuSurf	$14_{\pm 0.5}$ hours
VolRecon	$60_{\pm 5}$ seconds
UFORecon	$100_{\pm 5}$ seconds
2DGS	$10_{\pm 0.5}$ minutes
GauSurf	$2_{\pm 0.2}$ hours
FatesGS	$14_{\pm 0.5}$ minutes
Ours	$1_{\pm 0.05}$ second

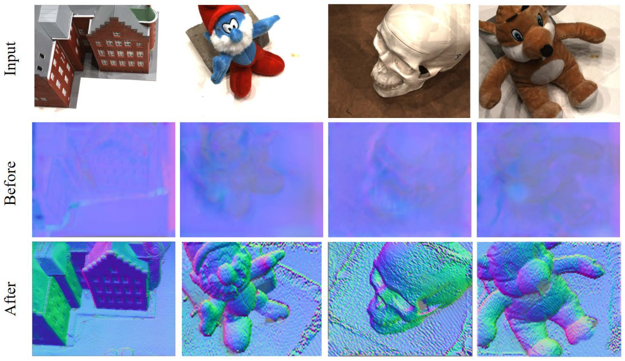

Figure 5: Visualization of Nyquist Theorem Verification

4.3 Experimental Nyquist Theorem Verifications

In Section 3.1, we analyze in detail how to derive the Nyquist sampling rates and spatial frequency of a Gaussian primitive. In our theoretical analysis, we prove that our surfel adaptation module can adjust the spatial frequency within Nyquist thresholds. To further demonstrate the effectiveness of our method, we conduct experiments on evaluated scenes for Nyquist criterion verification. We record the rendered depth maps and scale factor distributions from all tested scenes, and calculate the corresponding sampling rates and spatial frequencies. From the Nyquist criterion, we know that ν_k and $\hat{\nu}_{Nyquist} = \frac{\hat{\nu}_{sampling}}{2}$ must satisfy $\frac{\nu_{surfel}}{\hat{\nu}_{Nyquist}} < 1$, so we summarize the normalized frequency ratio $\frac{\nu_{surfel}}{\hat{\nu}_{Nyquist}}$ across all Gaussian surfels.

As illustrated in Figure 6, we can see that before surfel adaptation, almost all Gaussian primitives exceed the Nyquist threshold. The network cannot obtain sufficient information during the backpropagation stage and thus is unable to recover precise geometry. After the surfel adaptation module, all Gaussian primitives fall within the Nyquist frequency boundary. As shown in Figure 5, the rendered normal maps before and after the surfel adaptation module show significant differences, which further validates our method.

4.4 Ablation Studies

To demonstrate the necessity and effectiveness of our proposed components, we conducted experiments on DTU evaluation scenes to measure the impact of individual technical designs on reconstruction performance. The proposed modules are tested for ablation: the surfel adaptation module and the feature aggregation module. As shown in Table 3, in addition to the mean Chamfer Distance values, we also evaluate the normal rendering errors. For ground truth normal vectors, we utilize the normal maps provided by Gaussian Surfel [19]. We conduct experiments with 2 input views and render the normal maps on the same views. The results demonstrate that removing any of the proposed modules results in different performance degradation, confirming the effectiveness of each proposed component.

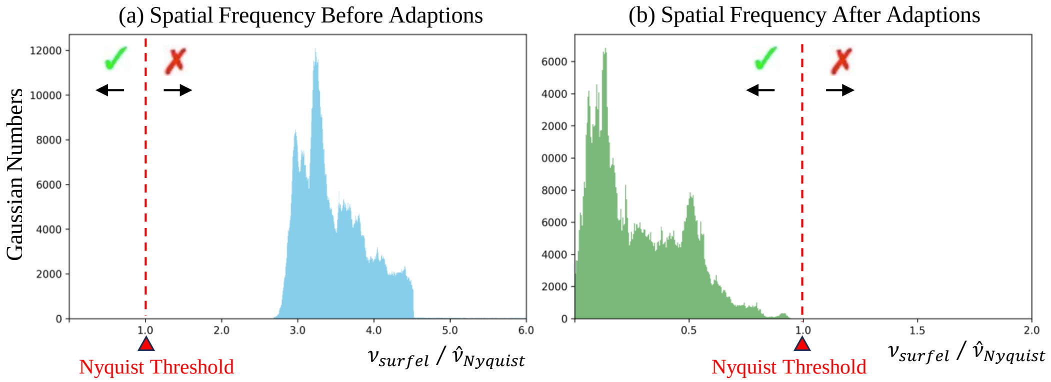

Figure 6: Nyquist Theorem Verification: (a) Before adaptation, most surfels exceed the Nyquist threshold, resulting in inaccurate geometry prediction. (b) After the adaptation module, all Gaussian primitives fall within the Nyquist threshold, ensuring accurate geometric feature learning.

Table 3: Ablation study of surfel adaption and feature aggregation module on DTU benchmarks.

Method	CD↓	Normal MSE↓
w/o Adaption.	2.56	0.135
w/o Aggre.	1.96	0.115
Ours	**1.12**	**0.060**

5 Conclusion and Discussion

In this paper, we propose SurfelSplat to predict surface-aligned Gaussian surfel representations from sparse-view images. To regress geometrically precise surfels, we apply Nyquist sampling criterion-guided surfel adaptation and feature aggregation modules to make the spatial frequency conform to the frequency constraints. Experimental results demonstrate that our method generates Gaussian radiance fields with more precise geometry and higher efficiency.

Although SurfaceSplat outperforms prior works, it has limitations. Since we predict pixel-aligned Gaussians for each view, the radiance fields are sensitive to image resolution. With higher resolutions such as 1024×1024, over 1 million Gaussian surfels would degrade both rendering and inference speed. Moreover, the unseen parts of the scene limit reconstruction performance, suggesting that generative models such as diffusion models could be introduced into our framework. Consequently, several promising directions remain to be explored.

We also acknowledge that the efficiency of our method benefits from the feed-forward architecture. However, integrating surface reconstruction effectively into feed-forward networks presents significant challenges: the orientations of Gaussian primitives cannot be correctly recovered due to insufficient spatial sampling frequency. To address this, we adopt surfel adaptation modules that enable each Gaussian primitive to acquire adequate geometric information, guided by the Nyquist sampling theorem, thereby achieving geometrically fine Gaussian radiance fields within the feed-forward framework.

Acknowledgments

This work was supported in part by the Beijing Natural Science Foundation under Grant L252011, and by the National Natural Science Foundation of China under Grant 62206147.

References

[1] Yao Yao, Zixin Luo, Shiwei Li, Tian Fang, and Long Quan. Mvsnet: Depth inference for unstructured multi-view stereo. In *Proceedings of the European conference on computer vision (ECCV)*, pages 767–783, 2018.

[2] Yikang Ding, Wentao Yuan, Qingtian Zhu, Haotian Zhang, Xiangyue Liu, Yuanjiang Wang, and Xiao Liu. Transmvsnet: Global context-aware multi-view stereo network with transformers. In *Proceedings of the IEEE/CVF conference on computer vision and pattern recognition*, pages 8585–8594, 2022.

[3] Peng Wang, Lingjie Liu, Yuan Liu, Christian Theobalt, Taku Komura, and Wenping Wang. Neus: Learning neural implicit surfaces by volume rendering for multi-view reconstruction. *arXiv preprint arXiv:2106.10689*, 2021.

[4] Lior Yariv, Jiatao Gu, Yoni Kasten, and Yaron Lipman. Volume rendering of neural implicit surfaces. *Advances in Neural Information Processing Systems*, 34:4805–4815, 2021.

[5] Zehao Yu, Songyou Peng, Michael Niemeyer, Torsten Sattler, and Andreas Geiger. Monosdf: Exploring monocular geometric cues for neural implicit surface reconstruction. *Advances in neural information processing systems*, 35:25018–25032, 2022.

[6] Han Huang, Yulun Wu, Junsheng Zhou, Ge Gao, Ming Gu, and Yu-Shen Liu. Neusurf: On-surface priors for neural surface reconstruction from sparse input views. In *Proceedings of the AAAI conference on artificial intelligence*, volume 38, pages 2312–2320, 2024.

[7] Xiaoxiao Long, Cheng Lin, Peng Wang, Taku Komura, and Wenping Wang. Sparseneus: Fast generalizable neural surface reconstruction from sparse views. In *European Conference on Computer Vision*, pages 210–227. Springer, 2022.

[8] Youngju Na, Woo Jae Kim, Kyu Beom Han, Suhyeon Ha, and Sung-Eui Yoon. Uforecon: generalizable sparse-view surface reconstruction from arbitrary and unfavorable sets. In *Proceedings of the IEEE/CVF Conference on Computer Vision and Pattern Recognition*, pages 5094–5104, 2024.

[9] Jiaming Sun, Yiming Xie, Linghao Chen, Xiaowei Zhou, and Hujun Bao. Neuralrecon: Real-time coherent 3d reconstruction from monocular video. In *2021 IEEE/CVF Conference on Computer Vision and Pattern Recognition (CVPR)*, 2021.

[10] Yiming Wang, Qin Han, Marc Habermann, Kostas Daniilidis, Christian Theobalt, and Lingjie Liu. Neus2: Fast learning of neural implicit surfaces for multi-view reconstruction. In *2023 IEEE/CVF International Conference on Computer Vision (ICCV)*, 2023.

[11] Haoyu Wu, Alexandros Graikos, and Dimitris Samaras. S-volsdf: Sparse multi-view stereo regularization of neural implicit surfaces. In *2023 IEEE/CVF International Conference on Computer Vision (ICCV)*, 2023.

[12] Lior Yariv, Jiatao Gu, Yoni Kasten, and Yaron Lipman. Volume rendering of neural implicit surfaces. In *Proceedings of the 35th International Conference on Neural Information Processing Systems*, 2021.

[13] Zhaoshuo Li, Thomas Müller, Alex Evans, Russell H. Taylor, Mathias Unberath, Ming-Yu Liu, and Chen-Hsuan Lin. Neuralangelo: High-fidelity neural surface reconstruction. In *2023 IEEE/CVF Conference on Computer Vision and Pattern Recognition (CVPR)*, 2023.

[14] Luoyuan Xu, Tao Guan, Yuesong Wang, Wenkai Liu, Zhaojie Zeng, Junle Wang, and Wei Yang. C2f2neus: Cascade cost frustum fusion for high fidelity and generalizable neural surface reconstruction. In *Proceedings of the IEEE/CVF International Conference on Computer Vision*, pages 18291–18301, 2023.

[15] Yixun Liang, Hao He, and Yingcong Chen. Retr: Modeling rendering via transformer for generalizable neural surface reconstruction. *Advances in neural information processing systems*, 36:62332–62351, 2023.

[16] Bernhard Kerbl, Georgios Kopanas, Thomas Leimkühler, and George Drettakis. 3d gaussian splatting for real-time radiance field rendering. *ACM Trans. Graph.*, 42(4):139–1, 2023.

[17] Antoine Guédon and Vincent Lepetit. Sugar: Surface-aligned gaussian splatting for efficient 3d mesh reconstruction and high-quality mesh rendering. In *Proceedings of the IEEE/CVF Conference on Computer Vision and Pattern Recognition*, pages 5354–5363, 2024.

[18] Binbin Huang, Zehao Yu, Anpei Chen, Andreas Geiger, and Shenghua Gao. 2d gaussian splatting for geometrically accurate radiance fields. In *ACM SIGGRAPH 2024 conference papers*, pages 1–11, 2024.

[19] Pinxuan Dai, Jiamin Xu, Wenxiang Xie, Xinguo Liu, Huamin Wang, and Weiwei Xu. High-quality surface reconstruction using gaussian surfels. In *ACM SIGGRAPH 2024 Conference Papers*, pages 1–11, 2024.

[20] Zehao Yu, Torsten Sattler, and Andreas Geiger. Gaussian opacity fields: Efficient adaptive surface reconstruction in unbounded scenes. *ACM Transactions on Graphics (TOG)*, 43(6):1–13, 2024.

[21] Mulin Yu, Tao Lu, Linning Xu, Lihan Jiang, Yuanbo Xiangli, and Bo Dai. Gsdf: 3dgs meets sdf for improved rendering and reconstruction. *arXiv preprint arXiv:2403.16964*, 2024.

[22] Stanislaw Szymanowicz, Chrisitian Rupprecht, and Andrea Vedaldi. Splatter image: Ultra-fast single-view 3d reconstruction. In *Proceedings of the IEEE/CVF conference on computer vision and pattern recognition*, pages 10208–10217, 2024.

[23] David Charatan, Sizhe Lester Li, Andrea Tagliasacchi, and Vincent Sitzmann. pixelsplat: 3d gaussian splats from image pairs for scalable generalizable 3d reconstruction. In *Proceedings of the IEEE/CVF conference on computer vision and pattern recognition*, pages 19457–19467, 2024.

[24] Yuedong Chen, Haofei Xu, Chuanxia Zheng, Bohan Zhuang, Marc Pollefeys, Andreas Geiger, Tat-Jen Cham, and Jianfei Cai. Mvsplat: Efficient 3d gaussian splatting from sparse multi-view images. In *European Conference on Computer Vision*, pages 370–386. Springer, 2024.

[25] Christopher Wewer, Kevin Raj, Eddy Ilg, Bernt Schiele, and Jan Eric Lenssen. latentsplat: Autoencoding variational gaussians for fast generalizable 3d reconstruction. In *European Conference on Computer Vision*, pages 456–473. Springer, 2024.

[26] Botao Ye, Sifei Liu, Haofei Xu, Xueting Li, Marc Pollefeys, Ming-Hsuan Yang, and Songyou Peng. No pose, no problem: Surprisingly simple 3d gaussian splats from sparse unposed images. *arXiv preprint arXiv:2410.24207*, 2024.

[27] Shengjun Zhang, Xin Fei, Fangfu Liu, Haixu Song, and Yueqi Duan. Gaussian graph network: Learning efficient and generalizable gaussian representations from multi-view images. *Advances in Neural Information Processing Systems*, 37:50361–50380, 2024.

[28] Shengji Tang, Weicai Ye, Peng Ye, Weihao Lin, Yang Zhou, Tao Chen, and Wanli Ouyang. Hisplat: Hierarchical 3d gaussian splatting for generalizable sparse-view reconstruction. *arXiv preprint arXiv:2410.06245*, 2024.

[29] Chuanrui Zhang, Yingshuang Zou, Zhuoling Li, Minmin Yi, and Haoqian Wang. Transplat: Generalizable 3d gaussian splatting from sparse multi-view images with transformers. *AAAI*, 2025.

[30] Ben Mildenhall, Pratul P Srinivasan, Matthew Tancik, Jonathan T Barron, Ravi Ramamoorthi, and Ren Ng. Nerf: Representing scenes as neural radiance fields for view synthesis. *Communications of the ACM*, 65(1):99–106, 2021.

[31] Jiawei Yang, Marco Pavone, and Yue Wang. Freenerf: Improving few-shot neural rendering with free frequency regularization. In *2023 IEEE/CVF Conference on Computer Vision and Pattern Recognition (CVPR)*, 2023.

[32] Anpei Chen, Zexiang Xu, Fuqiang Zhao, Xiaoshuai Zhang, Fanbo Xiang, Jingyi Yu, and Hao Su. Mvsnerf: Fast generalizable radiance field reconstruction from multi-view stereo. In *2021 IEEE/CVF International Conference on Computer Vision (ICCV)*, 2021.

[33] Jonathan T Barron, Ben Mildenhall, Matthew Tancik, Peter Hedman, Ricardo Martin-Brualla, and Pratul P Srinivasan. Mip-nerf: A multiscale representation for anti-aliasing neural radiance fields. In *ICCV*, pages 5855–5864, 2021.

[34] Christian Reiser, Songyou Peng, Yiyi Liao, and Andreas Geiger. Kilonerf: Speeding up neural radiance fields with thousands of tiny mlps. In *ICCV*, pages 14335–14345, 2021.

[35] Qiangeng Xu, Zexiang Xu, Julien Philip, Sai Bi, Zhixin Shu, Kalyan Sunkavalli, and Ulrich Neumann. Point-nerf: Point-based neural radiance fields. In *2022 IEEE/CVF Conference on Computer Vision and Pattern Recognition (CVPR)*, 2022.

[36] Stephan J Garbin, Marek Kowalski, Matthew Johnson, Jamie Shotton, and Julien Valentin. Fastnerf: High-fidelity neural rendering at 200fps. In *ICCV*, pages 14346–14355, 2021.

[37] Tao Hu, Shu Liu, Yilun Chen, Tiancheng Shen, and Jiaya Jia. Efficientnerf efficient neural radiance fields. In *CVPR*, pages 12902–12911, 2022.

[38] Mijeong Kim, Seonguk Seo, and Bohyung Han. Infonerf: Ray entropy minimization for few-shot neural volume rendering. In *2022 IEEE/CVF Conference on Computer Vision and Pattern Recognition (CVPR)*, 2022.

[39] Congyue Deng, Chiyu Max Jiang, Charles R. Qi, Xinchen Yan, Yin Zhou, Leonidas Guibas, and Dragomir Anguelov. Nerdi: Single-view nerf synthesis with language-guided diffusion as general image priors. In *2023 IEEE/CVF Conference on Computer Vision and Pattern Recognition (CVPR)*, 2023.

[40] Lingjie Liu, Jiatao Gu, Kyaw Zaw Lin, Tat-Seng Chua, and Christian Theobalt. Neural sparse voxel fields. *NeurIPS*, 33:15651–15663, 2020.

[41] Lars Mescheder, Michael Oechsle, Michael Niemeyer, Sebastian Nowozin, and Andreas Geiger. Occupancy networks: Learning 3d reconstruction in function space. In *2019 IEEE/CVF Conference on Computer Vision and Pattern Recognition (CVPR)*, 2019.

[42] Albert Pumarola, Enric Corona, Gerard Pons-Moll, and Francesc Moreno-Noguer. D-nerf: Neural radiance fields for dynamic scenes. In *CVPR*, pages 10318–10327, 2021.

[43] Linning Xu, Yuanbo Xiangli, Sida Peng, Xingang Pan, Nanxuan Zhao, Christian Theobalt, Bo Dai, and Dahua Lin. Grid-guided neural radiance fields for large urban scenes. In *CVPR*, pages 8296–8306, 2023.

[44] Haithem Turki, Deva Ramanan, and Mahadev Satyanarayanan. Mega-nerf: Scalable construction of large-scale nerfs for virtual fly-throughs. In *CVPR*, pages 12922–12931, 2022.

[45] Matthew Tancik, Vincent Casser, Xinchen Yan, Sabeek Pradhan, Ben Mildenhall, Pratul P Srinivasan, Jonathan T Barron, and Henrik Kretzschmar. Block-nerf: Scalable large scene neural view synthesis. In *CVPR*, pages 8248–8258, 2022.

[46] Haotong Lin, Sida Peng, Zhen Xu, Yunzhi Yan, Qing Shuai, Hujun Bao, and Xiaowei Zhou. Efficient neural radiance fields for interactive free-viewpoint video. In *SIGGRAPH Asia*, pages 1–9, 2022.

[47] Alex Yu, Vickie Ye, Matthew Tancik, and Angjoo Kanazawa. pixelnerf: Neural radiance fields from one or few images. In *CVPR*, pages 4578–4587, 2021.

[48] Yuanbo Xiangli, Linning Xu, Xingang Pan, Nanxuan Zhao, Anyi Rao, Christian Theobalt, Bo Dai, and Dahua Lin. Bungeenerf: Progressive neural radiance field for extreme multi-scale scene rendering. In *ECCV*, pages 106–122. Springer, 2022.

[49] Chen Gao, Ayush Saraf, Johannes Kopf, and Jia-Bin Huang. Dynamic view synthesis from dynamic monocular video. In *ICCV*, 2021.

[50] Zak Murez, Tarrence Van As, James Bartolozzi, Ayan Sinha, Vijay Badrinarayanan, and Andrew Rabinovich. Atlas: End-to-end 3d scene reconstruction from posed images. In *European conference on computer vision*, pages 414–431. Springer, 2020.

[51] Yufan Ren, Fangjinhua Wang, Tong Zhang, Marc Pollefeys, and Sabine Süsstrunk. Volrecon: Volume rendering of signed ray distance functions for generalizable multi-view reconstruction. In *Proceedings of the IEEE/CVF Conference on Computer Vision and Pattern Recognition*, pages 16685–16695, 2023.

[52] Jonathon Luiten, Georgios Kopanas, Bastian Leibe, and Deva Ramanan. Dynamic 3d gaussians: Tracking by persistent dynamic view synthesis. In *2024 International Conference on 3D Vision (3DV)*, 2024.

[53] Shunyuan Zheng, Boyao Zhou, Ruizhi Shao, Boning Liu, Shengping Zhang, Liqiang Nie, and Yebin Liu. Gps-gaussian: Generalizable pixel-wise 3d gaussian splatting for real-time human novel view synthesis. In *2024 IEEE/CVF Conference on Computer Vision and Pattern Recognition (CVPR)*, 2024.

[54] Zehao Yu, Anpei Chen, Binbin Huang, Torsten Sattler, and Andreas Geiger. Mip-splatting: Alias-free 3d gaussian splatting. In *Proceedings of the IEEE/CVF conference on computer vision and pattern recognition*, pages 19447–19456, 2024.

[55] Johannes L Schonberger and Jan-Michael Frahm. Structure-from-motion revisited. In *CVPR*, pages 4104–4113, 2016.

[56] Zhiwen Fan, Kevin Wang, Kairun Wen, Zehao Zhu, Dejia Xu, and Zhangyang Wang. Light-gaussian: Unbounded 3d gaussian compression with 15x reduction and 200+ fps. *arXiv preprint arXiv:2311.17245*, 2023.

[57] Tao Lu, Mulin Yu, Linning Xu, Yuanbo Xiangli, Limin Wang, Dahua Lin, and Bo Dai. Scaffold-gs: Structured 3d gaussians for view-adaptive rendering. *arXiv preprint arXiv:2312.00109*, 2023.

[58] Kai Katsumata, Duc Minh Vo, and Hideki Nakayama. An efficient 3d gaussian representation for monocular/multi-view dynamic scenes. *arXiv preprint arXiv:2311.12897*, 2023.

[59] Hanlin Chen, Chen Li, and Gim Hee Lee. Neusg: Neural implicit surface reconstruction with 3d gaussian splatting guidance. *arXiv preprint arXiv:2312.00846*, 2023.

[60] Harry Nyquist. Certain topics in telegraph transmission theory. *Transactions of the American Institute of Electrical Engineers*, 47(2):617–644, 2009.

[61] Henrik Aanæs, Rasmus Ramsbøl Jensen, George Vogiatzis, Engin Tola, and Anders Bjorholm Dahl. Large-scale data for multiple-view stereopsis. *International Journal of Computer Vision*, 120:153–168, 2016.

[62] Tinghui Zhou, Richard Tucker, John Flynn, Graham Fyffe, and Noah Snavely. Stereo magnification: Learning view synthesis using multiplane images. *arXiv preprint arXiv:1805.09817*, 2018.

[63] Yao Yao, Zixin Luo, Shiwei Li, Jingyang Zhang, Yufan Ren, Lei Zhou, Tian Fang, and Long Quan. Blendedmvs: A large-scale dataset for generalized multi-view stereo networks. In *Proceedings of the IEEE/CVF conference on computer vision and pattern recognition*, pages 1790–1799, 2020.

[64] Han Huang, Yulun Wu, Chao Deng, Ge Gao, Ming Gu, and Yu-Shen Liu. Fatesgs: Fast and accurate sparse-view surface reconstruction using gaussian splatting with depth-feature consistency. *arXiv preprint arXiv:2501.04628*, 2025.

[65] Hanspeter Pfister, Matthias Zwicker, Jeroen Van Baar, and Markus Gross. Surfels: Surface elements as rendering primitives. In *Proceedings of the 27th annual conference on Computer graphics and interactive techniques*, pages 335–342, 2000.

[66] Jianyuan Wang, Minghao Chen, Nikita Karaev, Andrea Vedaldi, Christian Rupprecht, and David Novotny. Vggt: Visual geometry grounded transformer. In *Proceedings of the Computer Vision and Pattern Recognition Conference*, pages 5294–5306, 2025.

[67] Shuzhe Wang, Vincent Leroy, Yohann Cabon, Boris Chidlovskii, and Jerome Revaud. Dust3r: Geometric 3d vision made easy. In *Proceedings of the IEEE/CVF Conference on Computer Vision and Pattern Recognition*, pages 20697–20709, 2024.

NeurIPS Paper Checklist

The checklist is designed to encourage best practices for responsible machine learning research, addressing issues of reproducibility, transparency, research ethics, and societal impact. Do not remove the checklist: **The papers not including the checklist will be desk rejected.** The checklist should follow the references and follow the (optional) supplemental material. The checklist does NOT count towards the page limit.

Please read the checklist guidelines carefully for information on how to answer these questions. For each question in the checklist:

- You should answer [Yes] , [No] , or [NA] .
- [NA] means either that the question is Not Applicable for that particular paper or the relevant information is Not Available.
- Please provide a short (1–2 sentence) justification right after your answer (even for NA).

The checklist answers are an integral part of your paper submission. They are visible to the reviewers, area chairs, senior area chairs, and ethics reviewers. You will be asked to also include it (after eventual revisions) with the final version of your paper, and its final version will be published with the paper.

The reviewers of your paper will be asked to use the checklist as one of the factors in their evaluation. While "[Yes] " is generally preferable to "[No] ", it is perfectly acceptable to answer "[No] " provided a proper justification is given (e.g., "error bars are not reported because it would be too computationally expensive" or "we were unable to find the license for the dataset we used"). In general, answering "[No] " or "[NA] " is not grounds for rejection. While the questions are phrased in a binary way, we acknowledge that the true answer is often more nuanced, so please just use your best judgment and write a justification to elaborate. All supporting evidence can appear either in the main paper or the supplemental material, provided in appendix. If you answer [Yes] to a question, in the justification please point to the section(s) where related material for the question can be found.

IMPORTANT, please:

- **Delete this instruction block, but keep the section heading "NeurIPS Paper Checklist"**,
- **Keep the checklist subsection headings, questions/answers and guidelines below.**
- **Do not modify the questions and only use the provided macros for your answers**.

1. **Claims**

   Question: Do the main claims made in the abstract and introduction accurately reflect the paper's contributions and scope?

   Answer: [Yes]

   Justification: We provide the main claims in the abstract and introduction.

   Guidelines:

   - The answer NA means that the abstract and introduction do not include the claims made in the paper.
   - The abstract and/or introduction should clearly state the claims made, including the contributions made in the paper and important assumptions and limitations. A No or NA answer to this question will not be perceived well by the reviewers.
   - The claims made should match theoretical and experimental results, and reflect how much the results can be expected to generalize to other settings.
   - It is fine to include aspirational goals as motivation as long as it is clear that these goals are not attained by the paper.

2. **Limitations**

   Question: Does the paper discuss the limitations of the work performed by the authors?

   Answer: [Yes]

   Justification: We discuss our limitations in the Appendix.

Guidelines:

- The answer NA means that the paper has no limitation while the answer No means that the paper has limitations, but those are not discussed in the paper.
- The authors are encouraged to create a separate "Limitations" section in their paper.
- The paper should point out any strong assumptions and how robust the results are to violations of these assumptions (e.g., independence assumptions, noiseless settings, model well-specification, asymptotic approximations only holding locally). The authors should reflect on how these assumptions might be violated in practice and what the implications would be.
- The authors should reflect on the scope of the claims made, e.g., if the approach was only tested on a few datasets or with a few runs. In general, empirical results often depend on implicit assumptions, which should be articulated.
- The authors should reflect on the factors that influence the performance of the approach. For example, a facial recognition algorithm may perform poorly when image resolution is low or images are taken in low lighting. Or a speech-to-text system might not be used reliably to provide closed captions for online lectures because it fails to handle technical jargon.
- The authors should discuss the computational efficiency of the proposed algorithms and how they scale with dataset size.
- If applicable, the authors should discuss possible limitations of their approach to address problems of privacy and fairness.
- While the authors might fear that complete honesty about limitations might be used by reviewers as grounds for rejection, a worse outcome might be that reviewers discover limitations that aren't acknowledged in the paper. The authors should use their best judgment and recognize that individual actions in favor of transparency play an important role in developing norms that preserve the integrity of the community. Reviewers will be specifically instructed to not penalize honesty concerning limitations.

3. **Theory assumptions and proofs**

   Question: For each theoretical result, does the paper provide the full set of assumptions and a complete (and correct) proof?

   Answer: [Yes]

   Justification: We provide assumptions and part of the proof in Section 3. The full proof can be found in the Appendix.

   Guidelines:

   - The answer NA means that the paper does not include theoretical results.
   - All the theorems, formulas, and proofs in the paper should be numbered and cross-referenced.
   - All assumptions should be clearly stated or referenced in the statement of any theorems.
   - The proofs can either appear in the main paper or the supplemental material, but if they appear in the supplemental material, the authors are encouraged to provide a short proof sketch to provide intuition.
   - Inversely, any informal proof provided in the core of the paper should be complemented by formal proofs provided in appendix or supplemental material.
   - Theorems and Lemmas that the proof relies upon should be properly referenced.

4. **Experimental result reproducibility**

   Question: Does the paper fully disclose all the information needed to reproduce the main experimental results of the paper to the extent that it affects the main claims and/or conclusions of the paper (regardless of whether the code and data are provided or not)?

   Answer: [Yes]

   Justification: We provide a detailed analysis of the theory and propose the network design and experimental details in Section 3, 4 and Appendix.

   Guidelines:

   - The answer NA means that the paper does not include experiments.

- If the paper includes experiments, a No answer to this question will not be perceived well by the reviewers: Making the paper reproducible is important, regardless of whether the code and data are provided or not.
- If the contribution is a dataset and/or model, the authors should describe the steps taken to make their results reproducible or verifiable.
- Depending on the contribution, reproducibility can be accomplished in various ways. For example, if the contribution is a novel architecture, describing the architecture fully might suffice, or if the contribution is a specific model and empirical evaluation, it may be necessary to either make it possible for others to replicate the model with the same dataset, or provide access to the model. In general. releasing code and data is often one good way to accomplish this, but reproducibility can also be provided via detailed instructions for how to replicate the results, access to a hosted model (e.g., in the case of a large language model), releasing of a model checkpoint, or other means that are appropriate to the research performed.
- While NeurIPS does not require releasing code, the conference does require all submissions to provide some reasonable avenue for reproducibility, which may depend on the nature of the contribution. For example
  (a) If the contribution is primarily a new algorithm, the paper should make it clear how to reproduce that algorithm.
  (b) If the contribution is primarily a new model architecture, the paper should describe the architecture clearly and fully.
  (c) If the contribution is a new model (e.g., a large language model), then there should either be a way to access this model for reproducing the results or a way to reproduce the model (e.g., with an open-source dataset or instructions for how to construct the dataset).
  (d) We recognize that reproducibility may be tricky in some cases, in which case authors are welcome to describe the particular way they provide for reproducibility. In the case of closed-source models, it may be that access to the model is limited in some way (e.g., to registered users), but it should be possible for other researchers to have some path to reproducing or verifying the results.

5. **Open access to data and code**

   Question: Does the paper provide open access to the data and code, with sufficient instructions to faithfully reproduce the main experimental results, as described in supplemental material?

   Answer: [No]

   Justification: We would like to release the codes if the submission is accepted.

   Guidelines:

   - The answer NA means that paper does not include experiments requiring code.
   - Please see the NeurIPS code and data submission guidelines (`https://nips.cc/public/guides/CodeSubmissionPolicy`) for more details.
   - While we encourage the release of code and data, we understand that this might not be possible, so “No” is an acceptable answer. Papers cannot be rejected simply for not including code, unless this is central to the contribution (e.g., for a new open-source benchmark).
   - The instructions should contain the exact command and environment needed to run to reproduce the results. See the NeurIPS code and data submission guidelines (`https://nips.cc/public/guides/CodeSubmissionPolicy`) for more details.
   - The authors should provide instructions on data access and preparation, including how to access the raw data, preprocessed data, intermediate data, and generated data, etc.
   - The authors should provide scripts to reproduce all experimental results for the new proposed method and baselines. If only a subset of experiments are reproducible, they should state which ones are omitted from the script and why.
   - At submission time, to preserve anonymity, the authors should release anonymized versions (if applicable).

- Providing as much information as possible in supplemental material (appended to the paper) is recommended, but including URLs to data and code is permitted.

6. **Experimental setting/details**

   Question: Does the paper specify all the training and test details (e.g., data splits, hyperparameters, how they were chosen, type of optimizer, etc.) necessary to understand the results?

   Answer: [Yes]

   Justification: We introduce the detailed experimental setup in Section 4.

   Guidelines:

   - The answer NA means that the paper does not include experiments.
   - The experimental setting should be presented in the core of the paper to a level of detail that is necessary to appreciate the results and make sense of them.
   - The full details can be provided either with the code, in appendix, or as supplemental material.

7. **Experiment statistical significance**

   Question: Does the paper report error bars suitably and correctly defined or other appropriate information about the statistical significance of the experiments?

   Answer: [Yes]

   Justification: We report 1-sigma error bars in Section 4.2 when comparing efficiency.

   Guidelines:

   - The answer NA means that the paper does not include experiments.
   - The authors should answer "Yes" if the results are accompanied by error bars, confidence intervals, or statistical significance tests, at least for the experiments that support the main claims of the paper.
   - The factors of variability that the error bars are capturing should be clearly stated (for example, train/test split, initialization, random drawing of some parameter, or overall run with given experimental conditions).
   - The method for calculating the error bars should be explained (closed form formula, call to a library function, bootstrap, etc.)
   - The assumptions made should be given (e.g., Normally distributed errors).
   - It should be clear whether the error bar is the standard deviation or the standard error of the mean.
   - It is OK to report 1-sigma error bars, but one should state it. The authors should preferably report a 2-sigma error bar than state that they have a 96% CI, if the hypothesis of Normality of errors is not verified.
   - For asymmetric distributions, the authors should be careful not to show in tables or figures symmetric error bars that would yield results that are out of range (e.g. negative error rates).
   - If error bars are reported in tables or plots, The authors should explain in the text how they were calculated and reference the corresponding figures or tables in the text.

8. **Experiments compute resources**

   Question: For each experiment, does the paper provide sufficient information on the computer resources (type of compute workers, memory, time of execution) needed to reproduce the experiments?

   Answer: [Yes]

   Justification: We provide the information in Section 4.

   Guidelines:

   - The answer NA means that the paper does not include experiments.
   - The paper should indicate the type of compute workers CPU or GPU, internal cluster, or cloud provider, including relevant memory and storage.

- The paper should provide the amount of compute required for each of the individual experimental runs as well as estimate the total compute.
- The paper should disclose whether the full research project required more compute than the experiments reported in the paper (e.g., preliminary or failed experiments that didn't make it into the paper).

9. **Code of ethics**

   Question: Does the research conducted in the paper conform, in every respect, with the NeurIPS Code of Ethics `https://neurips.cc/public/EthicsGuidelines`?

   Answer: [Yes]

   Justification: We reviewed the NeurIPS Code of Ethics carefully.

   Guidelines:

   - The answer NA means that the authors have not reviewed the NeurIPS Code of Ethics.
   - If the authors answer No, they should explain the special circumstances that require a deviation from the Code of Ethics.
   - The authors should make sure to preserve anonymity (e.g., if there is a special consideration due to laws or regulations in their jurisdiction).

10. **Broader impacts**

    Question: Does the paper discuss both potential positive societal impacts and negative societal impacts of the work performed?

    Answer: [Yes]

    Justification: We discuss potential social impacts in Appendix.

    Guidelines:

    - The answer NA means that there is no societal impact of the work performed.
    - If the authors answer NA or No, they should explain why their work has no societal impact or why the paper does not address societal impact.
    - Examples of negative societal impacts include potential malicious or unintended uses (e.g., disinformation, generating fake profiles, surveillance), fairness considerations (e.g., deployment of technologies that could make decisions that unfairly impact specific groups), privacy considerations, and security considerations.
    - The conference expects that many papers will be foundational research and not tied to particular applications, let alone deployments. However, if there is a direct path to any negative applications, the authors should point it out. For example, it is legitimate to point out that an improvement in the quality of generative models could be used to generate deepfakes for disinformation. On the other hand, it is not needed to point out that a generic algorithm for optimizing neural networks could enable people to train models that generate Deepfakes faster.
    - The authors should consider possible harms that could arise when the technology is being used as intended and functioning correctly, harms that could arise when the technology is being used as intended but gives incorrect results, and harms following from (intentional or unintentional) misuse of the technology.
    - If there are negative societal impacts, the authors could also discuss possible mitigation strategies (e.g., gated release of models, providing defenses in addition to attacks, mechanisms for monitoring misuse, mechanisms to monitor how a system learns from feedback over time, improving the efficiency and accessibility of ML).

11. **Safeguards**

    Question: Does the paper describe safeguards that have been put in place for responsible release of data or models that have a high risk for misuse (e.g., pretrained language models, image generators, or scraped datasets)?

    Answer: [NA]

    Justification: Our paper does not pose such risks.

    Guidelines:

    - The answer NA means that the paper poses no such risks.

- Released models that have a high risk for misuse or dual-use should be released with necessary safeguards to allow for controlled use of the model, for example by requiring that users adhere to usage guidelines or restrictions to access the model or implementing safety filters.
- Datasets that have been scraped from the Internet could pose safety risks. The authors should describe how they avoided releasing unsafe images.
- We recognize that providing effective safeguards is challenging, and many papers do not require this, but we encourage authors to take this into account and make a best faith effort.

12. **Licenses for existing assets**

    Question: Are the creators or original owners of assets (e.g., code, data, models), used in the paper, properly credited and are the license and terms of use explicitly mentioned and properly respected?

    Answer: [NA]

    Justification: Our paper does not use existing asserts.

    Guidelines:

    - The answer NA means that the paper does not use existing assets.
    - The authors should cite the original paper that produced the code package or dataset.
    - The authors should state which version of the asset is used and, if possible, include a URL.
    - The name of the license (e.g., CC-BY 4.0) should be included for each asset.
    - For scraped data from a particular source (e.g., website), the copyright and terms of service of that source should be provided.
    - If assets are released, the license, copyright information, and terms of use in the package should be provided. For popular datasets, `paperswithcode.com/datasets` has curated licenses for some datasets. Their licensing guide can help determine the license of a dataset.
    - For existing datasets that are re-packaged, both the original license and the license of the derived asset (if it has changed) should be provided.
    - If this information is not available online, the authors are encouraged to reach out to the asset's creators.

13. **New assets**

    Question: Are new assets introduced in the paper well documented and is the documentation provided alongside the assets?

    Answer: [NA]

    Justification: Our paper does not release new asserts.

    Guidelines:

    - The answer NA means that the paper does not release new assets.
    - Researchers should communicate the details of the dataset/code/model as part of their submissions via structured templates. This includes details about training, license, limitations, etc.
    - The paper should discuss whether and how consent was obtained from people whose asset is used.
    - At submission time, remember to anonymize your assets (if applicable). You can either create an anonymized URL or include an anonymized zip file.

14. **Crowdsourcing and research with human subjects**

    Question: For crowdsourcing experiments and research with human subjects, does the paper include the full text of instructions given to participants and screenshots, if applicable, as well as details about compensation (if any)?

    Answer: [NA]

    Justification: Our paper does not involve crowdsourcing nor research with human subjects.

Guidelines:

- The answer NA means that the paper does not involve crowdsourcing nor research with human subjects.
- Including this information in the supplemental material is fine, but if the main contribution of the paper involves human subjects, then as much detail as possible should be included in the main paper.
- According to the NeurIPS Code of Ethics, workers involved in data collection, curation, or other labor should be paid at least the minimum wage in the country of the data collector.

15. **Institutional review board (IRB) approvals or equivalent for research with human subjects**

    Question: Does the paper describe potential risks incurred by study participants, whether such risks were disclosed to the subjects, and whether Institutional Review Board (IRB) approvals (or an equivalent approval/review based on the requirements of your country or institution) were obtained?

    Answer: [NA]

    Justification: Our paper does not involve crowdsourcing nor research with human subjects.

    Guidelines:

    - The answer NA means that the paper does not involve crowdsourcing nor research with human subjects.
    - Depending on the country in which research is conducted, IRB approval (or equivalent) may be required for any human subjects research. If you obtained IRB approval, you should clearly state this in the paper.
    - We recognize that the procedures for this may vary significantly between institutions and locations, and we expect authors to adhere to the NeurIPS Code of Ethics and the guidelines for their institution.
    - For initial submissions, do not include any information that would break anonymity (if applicable), such as the institution conducting the review.

16. **Declaration of LLM usage**

    Question: Does the paper describe the usage of LLMs if it is an important, original, or non-standard component of the core methods in this research? Note that if the LLM is used only for writing, editing, or formatting purposes and does not impact the core methodology, scientific rigorousness, or originality of the research, declaration is not required.

    Answer: [NA]

    Justification: We utilize LLMs for grammar checking.

    Guidelines:

    - The answer NA means that the core method development in this research does not involve LLMs as any important, original, or non-standard components.
    - Please refer to our LLM policy (`https://neurips.cc/Conferences/2025/LLM`) for what should or should not be described.

Appendix

A Preliminaries

A.1 Surfels: Surface Elements

Surface elements, commonly referred to as *surfels*, constitute a point-based representation paradigm for modeling three-dimensional surfaces without explicit connectivity information. Originally introduced by Pfister et al. [65], surfels have emerged as a powerful alternative to traditional mesh-based representations in various surface reconstruction applications.

A surfel s is formally defined as a tuple:

$$s = \mathbf{p}, \mathbf{n}, r, \mathbf{c}, \sigma \tag{16}$$

where:

- $\mathbf{p} \in \mathbb{R}^3$ denotes the 3D position vector of the surfel
- $\mathbf{n} \in \mathbb{S}^2$ represents the unit normal vector ($\mathbb{S}^2$ being the unit sphere in $\mathbb{R}^3$)
- $r \in \mathbb{R}^+$ specifies the radius (or size) of the surfel
- $\mathbf{c} \in \mathbb{R}^3$ or $\mathbb{R}^4$ encodes color information (optional)
- $\sigma \in \mathbb{R}^+$ indicates the confidence or uncertainty measure (optional)

Each surfel can be geometrically interpreted as a local surface approximation, typically visualized as a oriented disk centered at $\mathbf{p}$ with radius r and orientation defined by $\mathbf{n}$. Collectively, a set of surfels $\mathcal{S} = s_1, s_2, ..., s_N$ forms a discrete sampling of the underlying continuous surface $\mathcal{M}$.

A.2 2D Gaussian Splatting

2D Gaussian splatting (2DGS) has demonstrated remarkable efficacy in achieving accurate and smooth surface extraction. Each 2D Gaussian primitive represents a tangent plane in 3D space characterized by three key parameters: a central position $\mathbf{p}_k$, two orthogonal tangential vectors $\mathbf{t}_u$ and $\mathbf{t}_v$, and a scaling vector $\mathbf{s} = (s_u, s_v)$ that determines the covariance of the 2D Gaussian primitive.

The normal vector of the surfel is computed as $\mathbf{t}_w = \mathbf{t}_u \times \mathbf{t}_v$. The rotation matrix is defined as $\mathbf{R} = [\mathbf{t}_u, \mathbf{t}_v, \mathbf{t}_w] \in \mathbb{R}^{3\times3}$, while the scaling vector is arranged into a diagonal scaling matrix $\mathbf{S} \in \mathbb{R}^{3\times3}$ with its last diagonal entry set to zero.

A point P in world space on the 2D Gaussian surfel p_k is defined in the local tangent space and parameterized by:

$$P(u, v) = \mathbf{p}_k + s_u\mathbf{t}_u u + s_v\mathbf{t}_v v = \mathbf{H}(u, v, 1, 1)^T \tag{17}$$

$$\mathbf{H} = \begin{bmatrix} s_u\mathbf{t}_u & s_v\mathbf{t}_v & \mathbf{0} & \mathbf{p}_k \\ 0 & 0 & 0 & 1 \end{bmatrix} = \begin{bmatrix} \mathbf{RS} & \mathbf{p}_k \\ \mathbf{0} & 1 \end{bmatrix} \tag{18}$$

where $\mathbf{H} \in \mathbb{R}^{4\times4}$ denotes the homogeneous transformation matrix. For a point $\mathbf{u} = (u, v)$ on the tangent plane, its Gaussian value is defined by: $\mathcal{G}(\mathbf{u}) = \exp\left(-\frac{u^2+v^2}{2}\right)$.

In this paper, we adopt the 2D Gaussian primitive as the fundamental surfel representation. The surfel attributes mentioned in Equation 16 can be mapped as follows: the center $\mathbf{p}$ corresponds to the central position $\mathbf{p}_k$; the normal vector is defined by $\mathbf{t}_w = \mathbf{t}_u \times \mathbf{t}_v$; the radius r is represented by the scaling vector $\mathbf{s} = (s_u, s_v)$; and the color $\mathbf{c}$ and uncertainty σ correspond to the spherical harmonic coefficients and opacity, respectively.

A.3 Spatial Fourier Transform

The Spatial Fourier Transform (SFT) provides a framework for analyzing spatial frequency components in multidimensional signals. For a continuous function $f(\mathbf{x})$ where $\mathbf{x} \in \mathbb{R}^d$ represents spatial coordinates in a d-dimensional space, the SFT is defined as:

$$\mathcal{F}\{f(\mathbf{x})\} = F(\mathbf{k}) = \int_{\mathbb{R}^d} f(\mathbf{x})e^{-i\mathbf{k}\cdot\mathbf{x}}d\mathbf{x} \tag{19}$$

where $\boldsymbol{\omega} \in \mathbb{R}^d$ denotes the spatial frequency vector and i is the imaginary unit. Correspondingly, the inverse SFT is expressed as:

$$\mathcal{F}^{-1}\{F(\mathbf{k})\} = f(\mathbf{x}) = \int_{\mathbb{R}^d} F(\mathbf{k}) e^{i\mathbf{k}\cdot\mathbf{x}} d\mathbf{k} \tag{20}$$

A.4 Basic Assumptions on the surface manifold

In the main body of our paper, the real signal we aim to recover is the 3D surface manifold of the scene. However, we only have access to discrete 2D image observations of this continuous 3D signal. And 2D Gaussian surfels are our chosen representation to approximate this surface.

Specifically, we model the real signal using a collection of 2D Gaussian primitives (following the foundation established by 2DGS [18] and Gaussian Surfels [19]). The problem of reconstructing the surface from discrete 2D sampling is thus reformulated as reconstructing the Gaussian primitives from the 2D image data.

B Mathematical Derivations

B.1 Spatial Sampling Rates in Multi-Camera Systems

In this paper, we provide a comprehensive derivation of the spatial sampling rates for a single-camera system. Intuitively, the spatial sampling interval in image space is unity, and the width and height of the sampling area are $\frac{f}{d}$ times larger than the spatial sampling interval of the image space. Therefore, we can readily derive the sampling frequency as $\frac{f_x f_y}{d^2}$.

Specifically, the spatial sampling rate $\hat{\nu}_{sampling}$ is determined by $\hat{\nu}_{sampling} = \frac{dA_{xy}}{dA_{uv}} = |\mathbf{J}|$, where $\mathbf{J}$ denotes the Jacobian matrix of the projection process. The projection process can be characterized by the following Jacobian matrix:

$$\mathbf{J} = \frac{\partial \mathbf{P}_{image}(x,y)}{\partial \mathbf{X}_{camera}} \cdot \frac{\partial \mathbf{X}_{camera}}{\partial \mathbf{X}_{world}} \cdot \frac{\partial \mathbf{X}_{world}}{\partial (u,v)} \tag{21}$$

First, a point in camera space X_C is derived from its corresponding point in world space X through the transformation: $X_C = RX + t$.

Subsequently, we project X_C onto the image plane, establishing the relationship between the point on the image plane $\mathbf{x}$ and X_C:

$$\mathbf{x} = \begin{pmatrix} x \\ y \end{pmatrix} = \begin{pmatrix} f_x \frac{X_C}{Z_C} + c_x \\ f_y \frac{Y_C}{Z_C} + c_y \end{pmatrix} \tag{22}$$

The corresponding Jacobian matrix can then be calculated as:

$$J_{2\times 3} = \frac{\partial \vec{x}}{\partial X} = \frac{\partial \vec{x}}{\partial X_C}\frac{\partial X_C}{\partial X} = \frac{1}{Z_C}\begin{pmatrix} f_x & 0 & -\frac{f_x}{Z_C} X_C \\ 0 & f_y & -\frac{f_y}{Z_C} Y_C \end{pmatrix} R \tag{23}$$

where Z_C represents the depth value $D(x,y)$ at the corresponding image coordinates. Analogously, the inverse transformation yields:

$$J_{3\times 2} = \frac{\partial X}{\partial X_C}\frac{\partial X_C}{\partial (u,v)} = R^T \frac{\partial X_C}{\partial (u,v)} = R^T \begin{pmatrix} 1 + \frac{u-c_x}{f_x}\frac{\partial Z_C}{\partial u} & \frac{u-c_x}{f_x}\frac{\partial Z_C}{\partial v} \\ \frac{v-c_y}{f_y}\frac{\partial Z_C}{\partial u} & 1 + \frac{v-c_y}{f_y}\frac{\partial Z_C}{\partial v} \\ \frac{\partial Z_C}{\partial u} & \frac{\partial Z_C}{\partial v} \end{pmatrix} \tag{24}$$

The overall Jacobian matrix is obtained through composition:

$$J = \frac{1}{Z_C}\begin{pmatrix} f_x & 0 & -\frac{f_x}{Z_C} X_C \\ 0 & f_y & -\frac{f_y}{Z_C} Y_C \end{pmatrix} RR^T \begin{pmatrix} 1 + \frac{u-c_x}{f_x}\frac{\partial Z_C}{\partial u} & \frac{u-c_x}{f_x}\frac{\partial Z_C}{\partial v} \\ \frac{v-c_y}{f_y}\frac{\partial Z_C}{\partial u} & 1 + \frac{v-c_y}{f_y}\frac{\partial Z_C}{\partial v} \\ \frac{\partial Z_C}{\partial u} & \frac{\partial Z_C}{\partial v} \end{pmatrix} = \begin{pmatrix} \frac{f_x}{Z_C} & 0 \\ 0 & \frac{f_y}{Z_C} \end{pmatrix} \tag{25}$$

Therefore, at point (x, y) on the image plane, the sampling rate for a single-camera system is:

$$\hat{\nu}_{sampling} = |J| = \frac{f_x f_y}{d^2} \tag{26}$$

where $d = Z_C(x, y)$. The overall sampling rate for a Gaussian primitive p_k is given by:

$$\hat{\nu}_k = \max\left(\{\mathbb{V}_i(p_k) \cdot |J_i|\}_{i=1}^{N}\right) \tag{27}$$

where N represents the number of cameras and $\mathbb{V}_i$ denotes the visibility function.

B.2 Spatial Frequency of a 2D Gaussian Primitive

Given a spatial geometry with an analytic mathematical expression, the spatial frequency can be computed through the Spatial Fourier Transform (SFT).

The three-dimensional Fourier transform of a 2D Gaussian basis element is given by:

$$\mathcal{G}(\mathbf{k}) = \int_{\mathbb{R}^3} \mathcal{G}(u, v)\delta(\mathbf{p} - (\mathbf{p}_k + s_u \mathbf{t}_u u + s_v \mathbf{t}_v v))e^{-i\mathbf{k}\cdot\mathbf{p}} d\mathbf{p} \tag{28}$$

Since the Gaussian primitive is confined to the tangent plane, the integral can be simplified to a two-dimensional parameter space:

$$\mathcal{G}(\mathbf{k}) = s_u s_v e^{-i\mathbf{k}\cdot\mathbf{p}_k} \int_{-\infty}^{\infty}\int_{-\infty}^{\infty} \exp\left(-\frac{u^2 + v^2}{2}\right) e^{-i(s_u \mathbf{t}_u \cdot \mathbf{k} \cdot u + s_v \mathbf{t}_v \cdot \mathbf{k} \cdot v)} du\, dv \tag{29}$$

Applying the two-dimensional Gaussian integral formula:

$$\int_{-\infty}^{\infty}\int_{-\infty}^{\infty} e^{-\frac{1}{2}(u^2+v^2) - i(au+bv)} du dv = 2\pi e^{-\frac{a^2+b^2}{2}} \tag{30}$$

where $a = s_u \mathbf{t}_u \cdot \mathbf{k}$ and $b = s_v \mathbf{t}_v \cdot \mathbf{k}$. Substituting these values yields:

$$\mathcal{G}(\mathbf{k}) = 2\pi s_u s_v e^{-i\mathbf{k}\cdot\mathbf{p}_k} \exp\left(-\frac{s_u^2(\mathbf{t}_u \cdot \mathbf{k})^2 + s_v^2(\mathbf{t}_v \cdot \mathbf{k})^2}{2}\right) \tag{31}$$

The spatial frequency spectrum of a 2D Gaussian surfel is therefore determined by:

$$|\hat{G}(\mathbf{k})| = 2\pi s_u s_v \exp\left(-\frac{s_u^2(\mathbf{k} \cdot \mathbf{t}_u)^2 + s_v^2(\mathbf{k} \cdot \mathbf{t}_v)^2}{2}\right) \tag{32}$$

We define the projection of the wave vector $\mathbf{k}$ onto the tangent vector $\mathbf{t}_u$ as the spatial frequency ν_u in that direction. Since the Gaussian function contains over 95% of its energy within ± 2 standard deviations, when considering a Gaussian of two standard deviations as the effective surfel size, the spatial frequency in the direction of $\mathbf{t}_u$ can be determined by the following condition:

$$-\frac{s_u^2(\mathbf{k} \cdot \mathbf{t}_u)^2 + s_v^2(\mathbf{k} \cdot \mathbf{t}_v)^2}{2} = -2, \quad \mathbf{k} \cdot \mathbf{t}_v = 0 \tag{33}$$

Thus, we obtain $\mathbf{t}_u \cdot \mathbf{k} = \frac{2}{s_u}$. Consequently, in the direction of $\mathbf{t}_u$, the angular frequency is $\omega_u = \mathbf{t}_u \cdot \mathbf{k} = \frac{2}{s_u}$ (and analogously, $\omega_v = \frac{2}{s_v}$ for the $\mathbf{t}_v$ direction).

Accounting for the 2π normalization convention of the Fourier transform, the spatial frequency of the Gaussian primitive along each tangent vector can be expressed as:

$$\nu_u = \frac{1}{\pi s_u}, \quad \nu_v = \frac{1}{\pi s_v} \tag{34}$$

C More Implementation Details and Experiments

C.1 Network Design

In the initial feature extraction network Φ_{image}, we implement a cross-view epipolar transformer and DINO feature backbones to extract preliminary image features $\mathcal{F}$. Subsequently, we employ the depth prediction network Φ_{depth} to regress per-view depth maps from the above image features. For the Gaussian feature prediction head Φ_{attr}, we utilize a 2D convolutional network. The feature refinement network Φ_{refine} is implemented via a cross-attention network as described in the original paper.

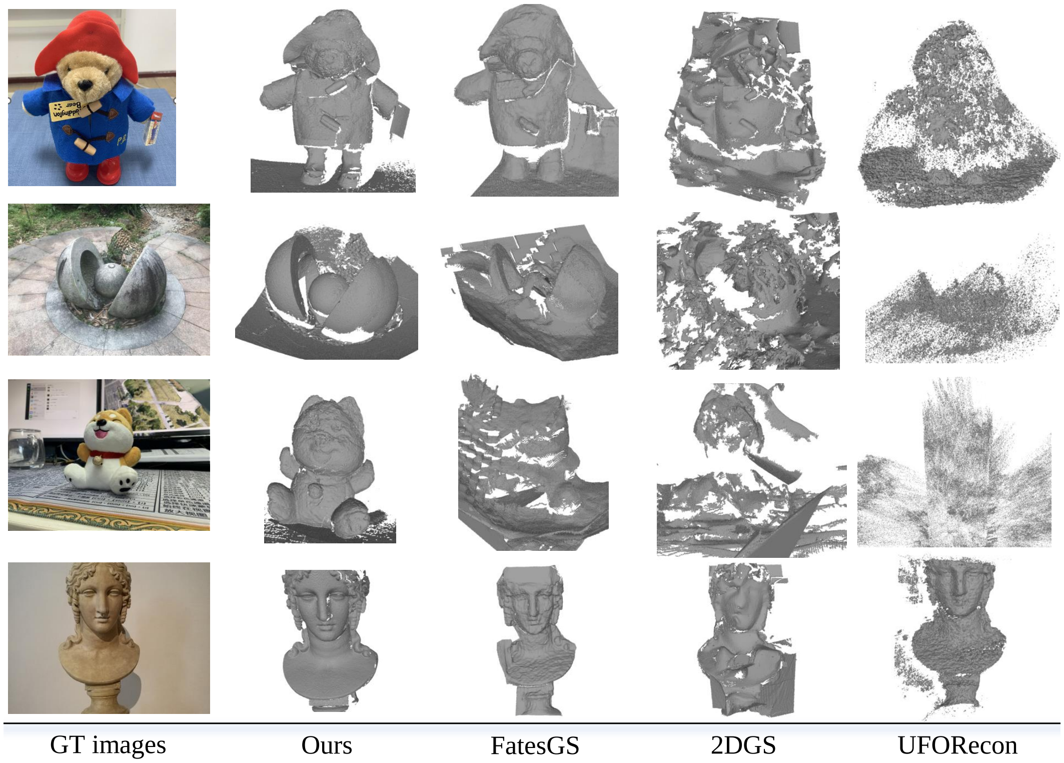

Figure 7: Visual comparison of 2-view reconstruction on BlendedMVS dataset.

C.2 Baselines

We compare our method with SOTA methods with 2 categories. **i.** Neural implicit methods: NeuS [3], VolRecon [51], UFORecon [8], NeuSurf [6]. **ii.** Neural Explicit methods: 2DGS [18], GausSurf [19], FatesGS [64].

C.3 Training Strategy

To progressively extract Gaussian features, we implement a two-phase curriculum learning-based training framework. During the initial phase, we leverage diverse scene datasets such as RealEstate10k [62]. Subsequently, in the refinement phase, we fine-tune the model on test sets from datasets such as DTU [61] that contain ground truth depth and surface measurements, thereby enhancing the precision of depth estimation and the characterization of geometric details.

C.4 Experiments on BlendedMVS

We conduct experiments on the BlendedMVS dataset [63] and visualize the qualitative results in Figure 7. Given a pair of images, our method exhibits consistent and stable performance across all tested scenes after fine-tuning. In contrast, methods such as UFORecon [8] cannot maintain consistent performance across different scenes and may produce significant geometric collapse in certain scenarios. FatesGS [64] and 2DGS [18] achieve stable performance, but they tend to suffer from insufficient geometric consistency and fail to converge to a complete and smooth surface.

C.5 Experiments on Novel View Synthesis

As shown in Figure 8, we further evaluate our approach through novel view synthesis experiments on the DTU dataset. Given a pair of input images, we synthesize intermediate viewpoints between the provided views and assess the quality of the generated novel views. We compare our method's visual fidelity against pixelSplat [23] and MVSplat [24]. To ensure a fair comparison, we fine-tune all baseline methods on the DTU training dataset and evaluate their performance on the designated

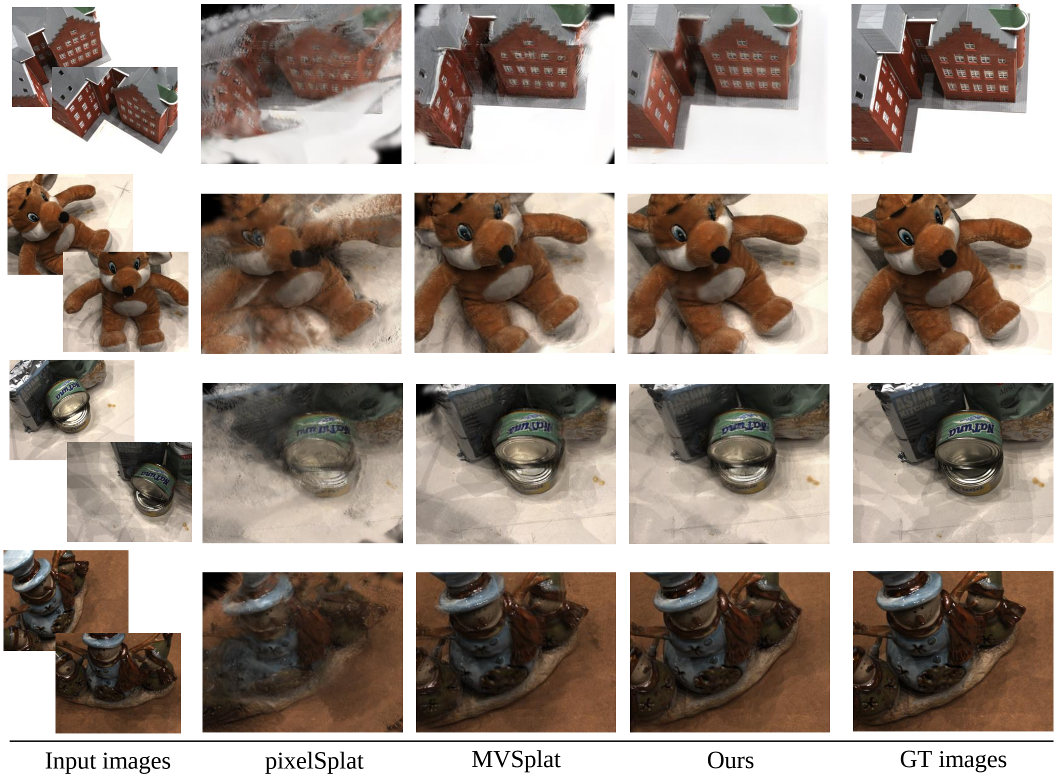

Figure 8: Visual comparison of novel view synthesis on DTU dataset.

test scenes. As demonstrated in Figure 8, our method achieves superior novel view synthesis quality compared to existing approaches. This improvement can be attributed to our method's ability to capture fine-grained geometric details that are not preserved by alternative techniques.

C.6 More Experimental Details

We constrain the Gaussian primitives to be either fully transparent or fully opaque, rather than semi-transparent. Consequently, the opacity attributes of 2D Gaussian Surfels are set to values approaching either 1 or 0 to facilitate clean surface extraction. The time consumption statistics reported in this paper represent the average inference time. The meshing process requires additional computational resources. On our hardware configuration, the meshing process consumes approximately 30 seconds.

D Broader Impacts

The proposed Gaussian feed-forward network approach for fast surface reconstruction carries several notable societal implications. First, the acceleration of reconstruction processes may democratize access to high-quality 3D modeling capabilities across resource-constrained environments, potentially reducing technological disparities between well-funded research institutions and those with limited computational infrastructure. We also recognize the environmental impact dimension. While our method reduces computational requirements per reconstruction task, the aggregate environmental effect depends on whether this efficiency leads to reduced energy consumption or, conversely, to increased utilization through rebound effects. Future work should quantify these energy consumption patterns to better understand the net environmental impact.

E Limitations and Future Works

Camera Pose Configuration. It is challenging for our approach to predict credible depth when input views only have small overlap regions. Our training data is relatively limited. We pretrain our method on Re10K dataset (about 10,000), and subsequently perform fine-tuning on the DTU dataset. Methods such as VGGT [66] and Dust3R [67] demonstrate robust depth prediction capabilities across a wide range of camera configurations, benefiting from extensive training data (more than 1,000,000) with explicit depth regularization. The generalizability of our method is not enough.

Efficiency. The cost-volume techique predicts depth by computing correspondence between pairs of images, which indicates that processing images requires computational operations. Additionally, our methodology directly combines Gaussian groups derived from different viewpoints to construct scene representations, resulting in redundant representations particularly in overlapping regions where similar Gaussian primitives are predicted from multiple source images. Besides, the pixel-aligned Gaussians are sensitive to the resolution of input images. For high resolution inputs, e.g. 1024×1024, we generate over 1 million Gaussians for each view, which will significantly increase the inference and rendering time. The consumption of computational resources and time grows rapidly with more views or higher resolutions.